

## Circular ultrasonic transducer characterization: theoretical and experimental results

L. Medina<sup>a</sup>, E. Moreno<sup>b</sup>, G. González<sup>c</sup>, and L. Leija<sup>c</sup>

<sup>a</sup>Departamento de Ingeniería de Sistemas Computacionales y Automatización, Instituto de Investigaciones en Matemáticas Aplicadas y Sistemas. UNAM, Circuito Escolar, Ciudad Universitaria, C.P. 04510, México D. F., México.

<sup>b</sup>Instituto de Cibernética, Matemática y Física (ICIMAF), La Habana Cuba.

<sup>c</sup>Sección de Bioelectrónica, Departamento de Ingeniería Eléctrica, CINVESTAV, Av. Instituto Politécnico Nacional 2508, C.P. 07360 México D.F.

Recibido el 30 de julio de 2002; aceptado el 9 de abril de 2003

Acoustic pressure fields generated by pulsed ultrasonic transducers under different boundary conditions are analyzed. Numerical simulations of the near-field pressure were evaluated considering rigid and soft baffles as boundary conditions. These field simulations were performed using the temporal convolution between the numerical derivative of the impulse response and the longitudinal wave velocity for both cases. Experimental pressure data were obtained by measuring the peak, peak to peak and root mean squared voltages. Simulated and experimental results were compared to investigate the temporal behavior of the acoustic signal as well as their spatial distribution on planes parallel to the transducer face. Special attention is given to the Fresnel region where the diffraction effect affects the pressure field measurements. Experimental readings were done using circular transducers with the same geometric characteristics and with resonant frequencies of 3.5 MHz and 5 MHz.

**Keywords:** Impulse response method; acoustic pressure distribution; ultrasonic transducer characterization.

En el presente trabajo se analiza la influencia de las condiciones de frontera en la distribución de presiones acústicas debido a la excitación impulsional de transductores ultrasónicos. Las simulaciones numéricas de la distribución de presiones en el campo cercano han sido desarrolladas considerando a los baffles rígido y suave como condiciones de frontera. Estos campos simulados han sido desarrollados en función de la convolución temporal entre la velocidad longitudinal de la cara del transductor y la derivada de la respuesta al impulso para ambas condiciones de frontera. Datos experimentales fueron obtenidos adquiriendo la señal eléctrica punto a punto y así obteniendo los voltajes pico, pico-pico y cuadrático medio. Los resultados experimentales y simulados son comparados para investigar el comportamiento temporal de las señales acústicas, así como sus distribuciones espaciales en planos paralelos a la superficie de los transductores. El experimento se enfocó en la región Fresnel donde el efecto de difracción, debido a los bordes de los transductores, afecta a la distribución de la presión acústica. Las lecturas experimentales fueron realizadas considerando transductores ultrasónicos circulares con las mismas características geométricas y frecuencias de resonancia de 3.5 MHz y 5 MHz.

**Descriptores:** Respuesta al impulso; campo de radiación acústica; caracterización de transductores.

PACS: 43.20.Bi; 43.25.Qp; 43.35.Yb

### 1. Introduction

An important feature of any ultrasonic instrumentation system is the transducer. This typically incorporates a piezoelectric element, which converts electrical signals into mechanical vibrations in the generation mode, and uses an inverse process for detection. Many ultrasonic applications involve transient or impulsive excitation of the active piezoelectric element. This extensive and varied range includes material characterization, non-destructive testing, biomedical imaging, tissue analysis and underwater viewing and position fixing system.

The ultrasonic field from such transducers is often the feature that determines the performance of a given system.

The study of the spatial and temporal characteristics of the acoustical pressure field allows a greater understanding of the behavior of such devices. It is an important tool to characterize and design ultrasonic transducers.

The acoustical pressure field analysis can be split into two regions: the near-field or Fresnel zone and the far-field or Fraunhofer zone [1]. These two acoustical regions are illustrated in Fig. 1.

The Fresnel zone, the region immediately in front of the transducer, is characterized by the rapid variations of the sound field due to the adding contribution of the direct waves and the diffracted edge waves [2]. The direct wave propagates in the geometrical beam region and the diffracted edge wave propagates in all directions from the edge of the transducer. The resultant field is then a function of the dimensions

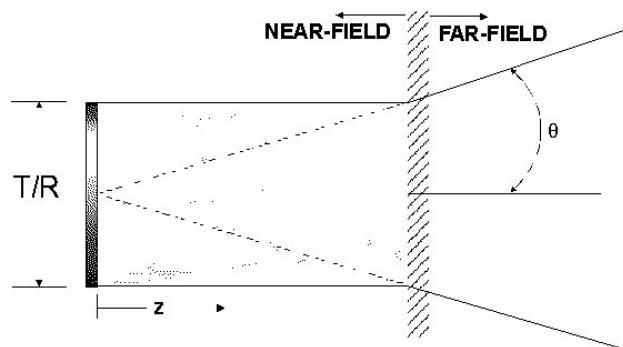


FIGURE 1. Near-field and Far-field regions of a transducer (T/R).

of the transducer and the transient motion of the transducer face.

The Fraunhofer zone is the region in which the radiated field decreases linearly with distance along a radial line connecting with the source [3].

Several methods have been developed to calculate the pressure field and used as guidelines for the design and characterization of transducer geometries [4]. The impulse response method [5, 6], which gives an exact solution for a transducer when considered as a planar piston, has proved to be a very powerful tool to predict the temporal and spatial acoustic pressure distribution in the regions in front of a transducer with specific geometric properties.

The impulse response is defined as a function of the velocity potential at an arbitrary spatial point resulting from an impulsive velocity motion of a piston. As a result of the transformation, an expression can be obtained for the impulse response as function of the spatial coordinates and time for any shape of piston radiator and also for different boundary conditions [6–8].

The aim of this work is to compare the transient fields radiated by pulsed ultrasonic transducers to those predicted by the impulse response theory. The considered boundary conditions are rigid, soft baffles and free-space.

The experimental and numerical estimates of the peak voltage, peak-peak voltage and root mean squared voltage are computed and compared. For that matter, both numerical and experimental pressure waveforms for specific points in space have been calculated.

Experimental readings have been carried out measuring the pressure field at specific points in space, focusing in the near field region of the transducers. Numerical measurements have been produced considering the experimental setup and boundary conditions. A comparison made between experimental and simulated data allowed to characterize the transducer behavior as rigid or soft baffle or as a combination of both boundary conditions.

## 2. Acoustic theory

The time-dependent acoustical pressure in the half-space  $z \geq 0$  (see Fig. 1), originated by the velocity of the piston vibrating in an isotropic medium, with constant velocity of propagation ( $c$ ), and assuming that the piston is mounted on an infinite planar baffle, can be formulated as a classical boundary value problem.

By choosing the appropriated boundary conditions to the wave equation for the velocity potential,  $\varphi(\mathbf{r}, t)$ , the emitted acoustic radiation is

$$\nabla^2 \varphi(\mathbf{r}, t) - \frac{1}{c^2} \frac{\partial^2 \varphi(\mathbf{r}, t)}{\partial t^2} = 0. \tag{1}$$

From Eq. (1) the acoustic pressure  $p(\mathbf{r}, t)$  can be obtained from

$$p(\mathbf{r}, t) = \rho_0 \frac{\partial \varphi(\mathbf{r}, t)}{\partial t}, \tag{2}$$

where  $\rho_0$  is the equilibrium density of the medium.

The time dependent velocity potential at an arbitrary observation point,  $\mathbf{r}$ , in the half space can be determined by

$$\varphi(\mathbf{r}, t) = \int_0^t dt_0 \int_S v(\mathbf{r}_0, t_0) g(|\mathbf{r} - \mathbf{r}_0|, t) dS, \tag{3}$$

where  $v(\mathbf{r}_0, t_0)$  is the piston face velocity,  $\mathbf{r}_0(x_0, y_0, z_0)$  is a point on the piston surface  $S$ , and  $g(|\mathbf{r} - \mathbf{r}_0|, t)$  is the Green's function of the a simple harmonic motion, dependent on the boundary conditions.

If the velocity is considered uniform over the piston face, and the Green's function is the solution of a pulse wave [9], then the velocity potential can be written as

$$\begin{aligned} \varphi(\mathbf{r}, t) &= \int_0^t v(t_0) dt_0 \int_S g(|\mathbf{r} - \mathbf{r}_0|, t) dS \\ &= v(t) * h(\mathbf{r}, t), \end{aligned} \tag{4}$$

where  $v(t)$  is the mean velocity at the piston face, the operation  $*$  represents the temporal convolution and  $h(\mathbf{r}, t)$  is defined as the impulse response function,

$$h(\mathbf{r}, t) = \int_S g(|\mathbf{r} - \mathbf{r}_0|, t) dS. \tag{5}$$

The impulse response depends on the boundary conditions and the transducer geometry.

Substituting Eq. (4) in Eq. (2), the acoustic pressure becomes

$$p(\mathbf{r}, t) = \rho_0 \frac{\partial}{\partial t} (v(t) * h(\mathbf{r}, t)) = \rho_0 \frac{\partial}{\partial t} v(t) * \frac{\partial h(\mathbf{r}, t)}{\partial t}. \tag{6}$$

The spatial component due to the diffraction effect can be separated from the temporal component produced by the piston face vibration using the impulse response method. This implies that the vibration amplitude at a certain point on the surface does not depend on time and the amplitude of the vibration, therefore is not influenced by the shape of the excitation.

### 2.1. Boundary conditions

In this work, we used the common boundary conditions [10–12]:

- a) Free-space. When the baffle matches the properties of the propagation medium, then the acoustic impedance of the medium is equal to the acoustic impedance of the baffle, and the fields are continuous across the boundary interface. The best-suited Green's function of the outgoing fundamental solution is

$$2g(|\mathbf{r} - \mathbf{r}_0|, t) = \frac{e^{i(\omega t - \mathbf{k} \cdot (\mathbf{r} - \mathbf{r}_0))}}{4\pi |\mathbf{r} - \mathbf{r}_0|}, \tag{7}$$

where  $\omega$  is the angular frequency of the vibrating source and  $\mathbf{k}$  is the wave-vector.

- b) Rigid baffle. If a piston is embedded on an infinite rigid baffle the only part able to vibrate is the piston face, it means that the normal velocity must go to zero on the boundary. The Green's function for this condition is given by

$$g(\mathbf{r}, t) = g(|\mathbf{r} - \mathbf{r}_0|, t) + g(|\mathbf{r} - \mathbf{r}_0 - 2\mathbf{z}|, t), \quad (8)$$

where  $z$  is the normal distance from the piston face to the observation point.

- c) Soft baffle. The acoustical potential must be zero at the boundary, then the pressure at  $z_0 = 0$  is zero outside the transducer surface. An appropriate Green's function can be

$$g(\mathbf{r}, t) = g(|\mathbf{r} - \mathbf{r}_0|, t) - g(|\mathbf{r} - \mathbf{r}_0 - 2\mathbf{z}|, t). \quad (9)$$

**2.2. Impulse response for a circular transducer:  $h(\mathbf{r}, t)$**

In order to evaluate the acoustic pressure, the impulse response for a particular geometry must be determined. The impulse response for a circular transducer of radius  $a$ , located at  $z_0 = 0$  embedded on an infinite rigid baffle, was first obtained by Obberhettinger (1961) [7], who noted that the response to an arbitrary excitation could be obtained by convolution. Stepanishen (1971) [5] pointed out that the impulse response of any baffled piston could be obtained by calculating the length of the circular arc on the piston face whose impulse radiation would arrive at each instant of time in-phase at a given field point. The impulse response when the piston is immersed on an infinite rigid baffle is stated as follows:

$$h_{rb}(\mathbf{r}, t) = \begin{cases} 0 & t < t_1, \\ c & t_1 \leq t < t_2, \\ \frac{c}{\pi} \cos^{-1} \left( \frac{r_{xy}^2 + (ct)^2 - z^2 - a^2}{2r_{xy}((ct)^2 - z^2)^{1/2}} \right) & t_2 \leq t \leq t_3, \\ 0 & t > t_3. \end{cases} \quad (10)$$

where  $r_{xy}$  is the projection of  $\mathbf{r}$  into the transducer plane. The temporal limits are given in Table I, which depend on the position of  $r_{xy}$ , as shown in Fig. 2.

The impulse response of a circular transducer for a soft baffle as a boundary condition, at which the normal stress is zero at  $z_0 = 0$  and outside the transducer, corresponds to the analysis of the diffraction given by the Rayleigh-Sommerfeld [9] surface integral. Rodríguez and co-workers [12] proposed an impulse response with soft baffle boundary conditions as follows:

$$h_{sb}(\mathbf{r}, t) = \begin{cases} 0 & t < t_1, \\ \frac{z}{t} + \int_{t_1}^t \frac{z}{t^2} dt & t_1 \leq t < t_2, \\ \frac{z}{t\pi} \cos^{-1} \left( \frac{r_{xy}^2 + (ct)^2 - z^2 - a^2}{2r_{xy}((ct)^2 - z^2)^{1/2}} \right) + \int_{t_1}^{t_2} \frac{z}{t^2} dt + \int_{t_2}^t \frac{z}{t^2\pi} \cos^{-1} \left( \frac{r_{xy}^2 + (ct)^2 - z^2 - a^2}{2r_{xy}((ct)^2 - z^2)^{1/2}} \right) dt & t_2 \leq t \leq t_3, \\ \int_{t_1}^{t_2} \frac{z}{t^2} dt + \int_{t_2}^{t_3} \frac{z}{t^2\pi} \cos^{-1} \left( \frac{r_{xy}^2 + (ct)^2 - z^2 - a^2}{2r_{xy}((ct)^2 - z^2)^{1/2}} \right) dt & t > t_3. \end{cases} \quad (11)$$

After dimensional analysis of Eq. (11), we can observe a disagreement for the impulse response when  $t > t_3$ . We introduced this correction and reformulated Eq. (11) as follows:

$$h_{sb}(\mathbf{r}, t) = \begin{cases} 0 & t < t_1, \\ \frac{z}{t} + \int_{t_1}^t \frac{z}{t^2} dt & t_1 \leq t < t_2, \\ \frac{z}{t\pi} \cos^{-1} \left( \frac{r_{xy}^2 + (ct)^2 - z^2 - a^2}{2r_{xy}((ct)^2 - z^2)^{1/2}} \right) + \int_{t_1}^{t_2} \frac{z}{t^2} dt + \int_{t_2}^t \frac{z}{t^2\pi} \cos^{-1} \left( \frac{r_{xy}^2 + (ct)^2 - z^2 - a^2}{2r_{xy}((ct)^2 - z^2)^{1/2}} \right) dt & t_2 \leq t \leq t_3, \\ \int_{t_1}^{t_2} \frac{z}{t^2} dt + \int_{t_2}^{t_3} \frac{z}{t^2\pi} \cos^{-1} \left( \frac{r_{xy}^2 + (ct)^2 - z^2 - a^2}{2r_{xy}((ct)^2 - z^2)^{1/2}} \right) dt & t > t_3. \end{cases} \quad (12)$$

when the transducer plane coincides with the  $xy$ -plane, then  $z_0 = 0$ , the Green's function for a rigid baffle becomes  $g(\mathbf{r}, t) = 2g(|\mathbf{r} - \mathbf{r}_0|, t)$  and a soft baffle is zero, then the free-space can be defined as the arithmetic mean between the rigid baffle and the soft baffle solutions.

TABLE I. Temporal limits for numerical evaluation of  $h(\mathbf{r}, t)$ .

$i)r_{xy} \leq a$	$ii)r_{xy} > a$
$t_1 = \frac{z}{c}$	$t_1 = t_2$
$t_2 = \frac{(z^2 + (a - r_{xy})^2)^{1/2}}{c}$	
$t_3 = \frac{(z^2 + (a + r_{xy})^2)^{1/2}}{c}$	

### 3. Simulation of the impulse response

To investigate the spatial and temporal pressure distributions due to the excitation of a circular transducer, it is necessary to study its impulse response considering the transducer geometry and specific boundary conditions. To simulate the impulse response of circular transducers, MATLAB programs were written based on rigid-and-soft baffles boundary conditions [Eq. (10) and Eq. (12)]. The velocity of the piston surface used in this process was experimentally acquired. The temporal evaluation of the impulse response was varied at certain steps depending on the sampling rate, until the distance of interest was fully covered. The pressure field distribution ( $P_c[n]$ ) for a number of points in the half-space, was calculated using Eq. 6. Some of the important parameters which can be derived from a pressure waveform are: a) the peak acoustic pressure ( $P_p$ ), defined as the maximum positive ( $p_+$ ) or maximum of the modulus of the negative ( $p_-$ ) instantaneous acoustic pressure, b) the peak to peak acoustic pressure ( $P_{pp}$ ) defined by the modulus of the difference between the maximum and minimum of the instantaneous acoustic pressure and c) the root mean squared of the instantaneous acoustic pressure ( $P_{rms}$ ) at a particular point in an acoustic field.

These parameters can be calculated as follows:

$$P_p = p_+ \quad \text{or} \quad P_p = |p_-|, \quad P_{pp} = |p_+ - p_-|,$$

$$P_{rms} = \sqrt{\frac{1}{N} \sum_{n=1}^N (P_c[n])^2}, \quad (13)$$

$P_p$  and  $P_{pp}$  are parameters related to the acoustic pressure intensity, and a very important tool for ultrasonic imaging, while the  $P_{rms}$  measurements correspond to the power of the pressure field at a specific point and a useful measurement to determine the ultrasonic dosimetry.

### 4. Materials and methods

The experimental work was carried out with a Hydrophone scanning system (Specialty Engineering Associates SEA), two Personal computers, and a digital oscilloscope (TDS-340 Tektronix). A schematic of the experimental set up is shown in Fig. 3.

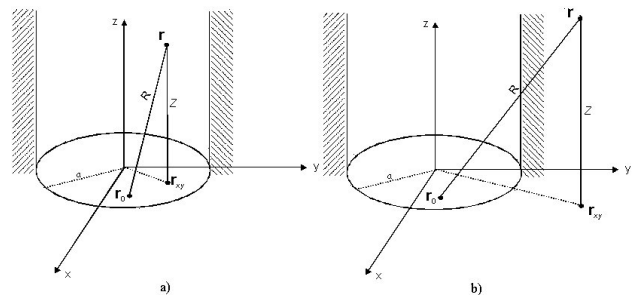


FIGURE 2. The projection of  $\mathbf{r}$ : a)  $r_{xy}$  inside and b)  $r_{xy}$  outside of the transducer surface.

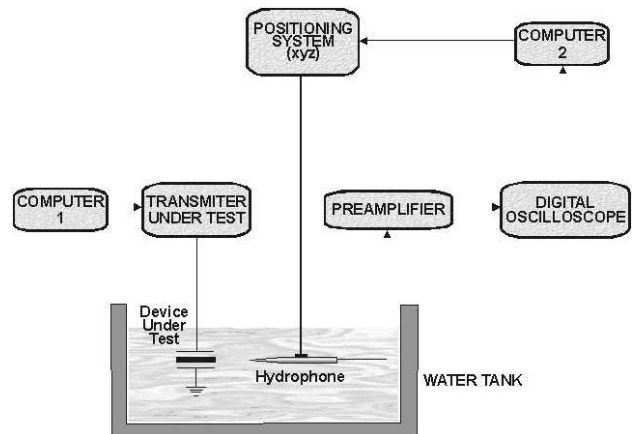


FIGURE 3. Ultrasonic scanning system with a water tank of size  $70 \times 20 \times 15cm_3$ .

This system is able to control a motor to move the hydrophone (PZT-Z44-0400) along the  $x - axis$ ,  $y - axis$  and  $z - axis$  with a  $10\mu m$  step. The system is also able to store the waveforms, calculate the parameters and display a graphical representation of the experimental data .

In a typical experiment, the transducer and the hydrophone are immersed in a water tank, then an ultrasonic transducer is excited producing a pulse, the computer-controlled motor moves the hydrophone point by point, and a oscilloscope records the corresponding signal from each point and stored. The transmission and triggering of the ultrasonic pulse of the transducer under test were controlled via a pulse-eco card MATEC SR9000.

The experimental scanning area is delimited to the near field of the tested transducers by the  $z - axis$ , which corresponds to the beam axis of the transducer, and the  $x - axis$  is an arbitrary axis normal to it.

The characteristics of the two ultrasonic transducers under test, commonly used in a non-destructive testing operation immersed in water, are given in Table II.

The sampling rate used in these experiments is 100 MHz and the velocity of propagation in water is approximately to  $c = 1500$  m/s.

TABLE II. Transducer Characteristics: resonant frequency  $f$  and radius  $a$

Panametrics	$f$ [MHz]	$a$ [mm]	Type
1	3.5	4.76	V383-SU
2	5.0	4.76	V326S

**5. Results and discussion**

The acoustic pressure distribution defined by Eq. (6) depends on the velocity at the face of the transducer and the derivative of the impulse response for a specific boundary condition. The velocity of the transducer face is calculated as an average of signals acquired at a plane parallel to the vibrating surface, at a normal distance of 0.5 mm from it. The velocity of each transducer, used in the simulation, is shown in Fig. 4.

The computed and experimental pressure distributions were obtained by scanning the  $x$  - axis, covering the effective

aperture at certain normal distances from the transducer plane, within the Fresnel limit ( $z_F$ ) [1] given by

$$z_F = \frac{a^2}{\lambda} = a^2 \frac{f}{c}, \tag{14}$$

where  $\lambda$  is the wavelength.

The Fresnel limit [Eq. (14)], for the transducer operating at 3.5 MHz is 52.9 mm and for the 5 MHz resonant frequency is 75.60 mm. The chosen normal distances within the Fresnel zone, to compare numerical and experimental data were 1 mm, 7 mm and 45 mm for the first transducer and 1.5 mm, 20 mm and 41mm for the other. The  $x$  position varied from -5.5 mm to 5.5 mm covering the transducer effective area.

**5.1. Circular transducer at 3.5 MHz of resonant frequency**

Theoretical pressure waveforms were calculated and then  $P_p, P_{pp}$  and  $P_{rms}$  were computed. Numerical data and experimental readings are shown from Fig. 5 to Fig. 7, respectively.

*5.1.1. Peak acoustic pressure*

In the first column of Fig. 5 (Figs. 5a, 5b and 5c), shows that the experimental readings have no uniform profile as sketched by the soft baffle situation (Fig. 5b) or two main lobes at the outermost points of the effective area of the transducer, as shown in Fig. 5a. However an overall amplitude of the experimental data is within 0.15, which is closer to the soft baffle pressure distribution calculations.

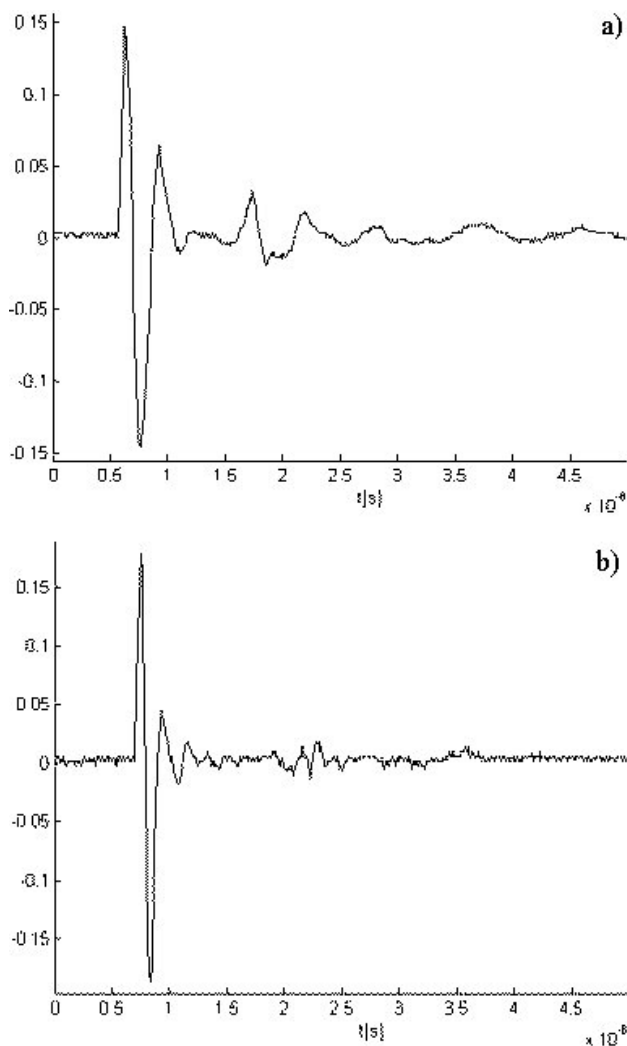


FIGURE 4. Face Velocity: a) 3.5 MHz and b) 5 MHz, transducer frequencies.

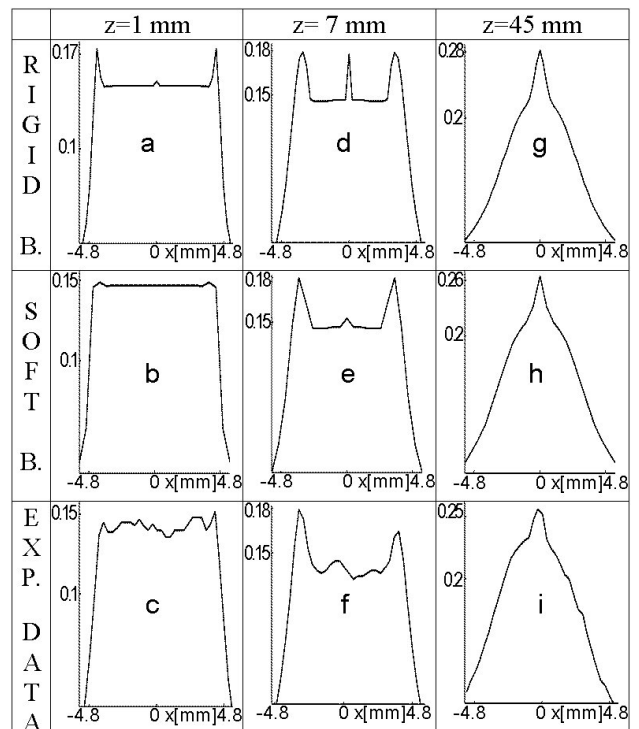


FIGURE 5. Theoretical and experimental results of  $P_p$  parameter for 3.5MHz transducer.

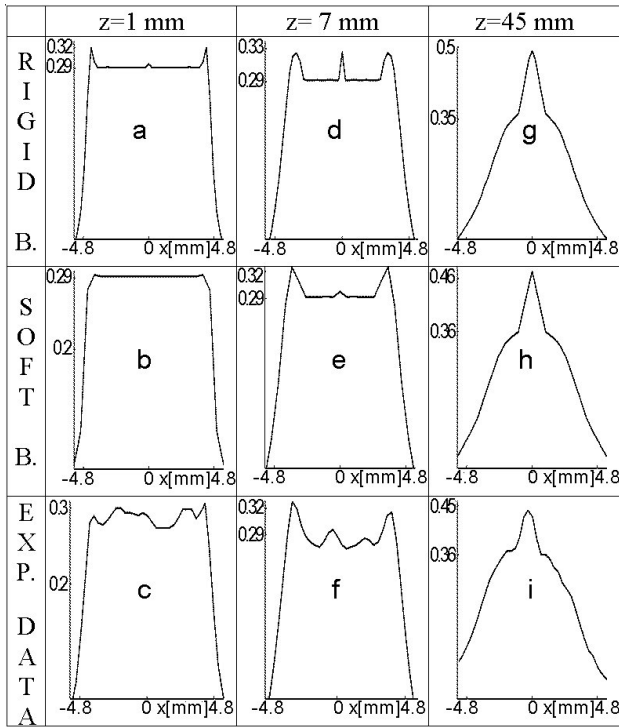


FIGURE 6. Theoretical values and experimental readings of  $P_{pp}$  parameter of a 3.5MHz transducer.

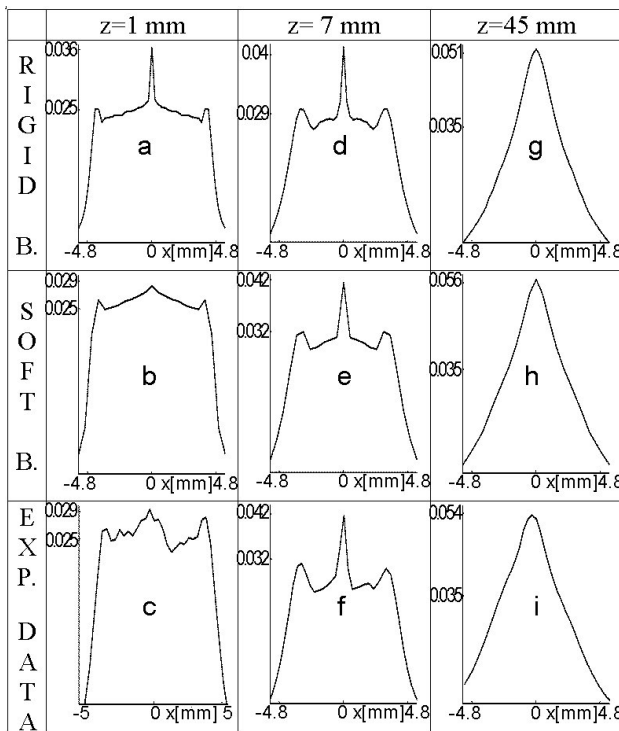


FIGURE 7. Theoretical and experimental  $P_{rms}$  parameter calculations of a 3.5MHz transducer.

In the second column (Figs. 5d, 5e and 5f), we can see that the main difference between the rigid and soft baffle conditions is found at  $x = 0$ , where the contribution of the direct wave is attenuated by the edge wave for the second case (see

Fig 5e). The experimental pressure distribution, at  $z = 7$  mm, consists of two main lobes at the same position of the one calculated for the soft baffle case, and a minor lobe close to  $x = 0$ .

And the last column plots the numerical and experimental pressure distributions close to the Fresnel limit. The differences between the numerical calculations (see Figs. 5g and 5h) is the amplitude at  $x = 0$ , and the length of the narrower peak. Experimental pressure distributions show a good agreement with the numerical distribution when a piston is immersed in a soft baffle, since its maximum value is about the same and has a very short peak length.

5.1.2. Peak-to-peak acoustic pressure

The peak-to-peak measurements contribute on the increment of the pressure intensity at any point. However the distribution profile (see Fig. 6) itself is similar to the plots shown in the last section. The amplitude and the profile of the experimental pressure distributions, at different normal distances from the transducer plane, show a good agreement with the numerical values computed considering the transducer to be immersed on an infinite soft baffle.

5.1.3. Root mean squared acoustic pressure

The  $P_{rms}$  measurements represent the power of the transducer at any region, therefore produces a different profile from the other two parameters.

Figure 7 plots the power of the numerical and experimental pressure distribution. It is worth noticing that the power is very low, since this transducer is for imaging purposes. The comparison between numerical values produced by the two boundary conditions, when the observation point is at  $z = 1$  mm, is that the power of the first boundary condition (see Fig. 7a) is concentrated at  $x = 0$ , while in the second boundary condition (see Fig. 7b) is at  $x \approx \pm a$ , and increasing smoothly until reaches its maximum at  $x = 0$ . The experimental data coincides to the second boundary condition, because of the maximum amplitude value and the amplitude difference between the power at  $x \approx \pm a$  and at  $x = 0$  (see Fig. 7c).

5.2. Circular transducer at 5 MHz of resonant frequency

Numerical pressure waveforms were produced and then  $P_p$ ,  $P_{pp}$  and  $P_{rms}$  were computed from them. Numerical and experimental readings are shown from Fig. 8 to Fig. 10.

5.2.1. Peak acoustic pressure

Numerical pressure distribution intensities produced by both boundary conditions are similar, when the observation point is at  $z = 1.5$  mm and  $z = 20$  mm (shown in Figs. 8a, 8b, 8d and 8e), with the exception of a small increment at  $x = 0$  for the rigid baffle (see Figs. 8a and 8d) and the maximum amplitude value is lower for the soft baffle case.

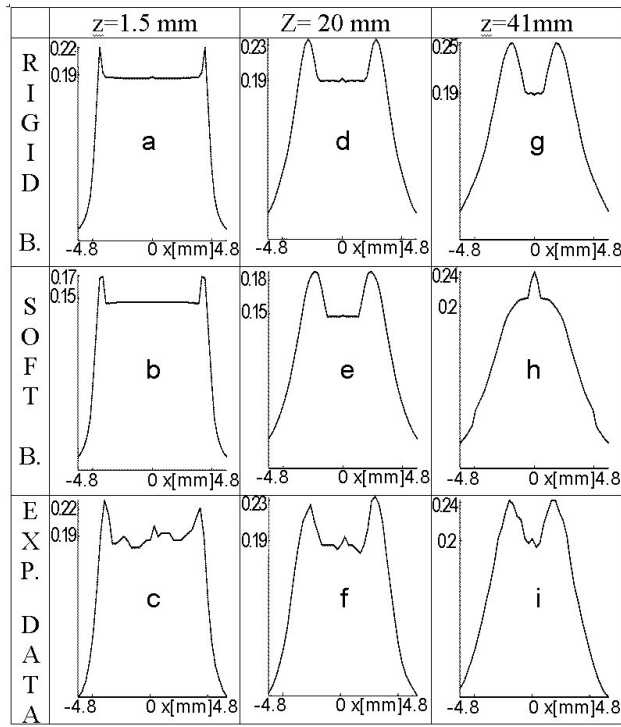


FIGURE 8. Theoretical and experimental results of  $P_p$  parameter for a 5 MHz transducer.

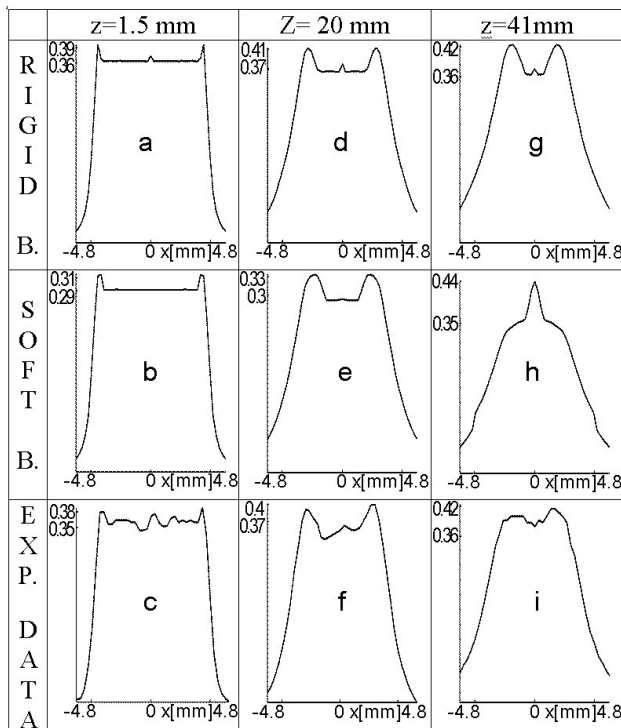


FIGURE 9. Theoretical values and experimental readings of  $P_{pp}$  parameter of a 5 MHz transducer.

Experimental intensities, measured at these observation points (shown in Figs. 8c, and 8f), have the following similar characteristics respect to the rigid baffle situation: a) the maximum intensities, b) an intensity increment around  $x = 0$  mm

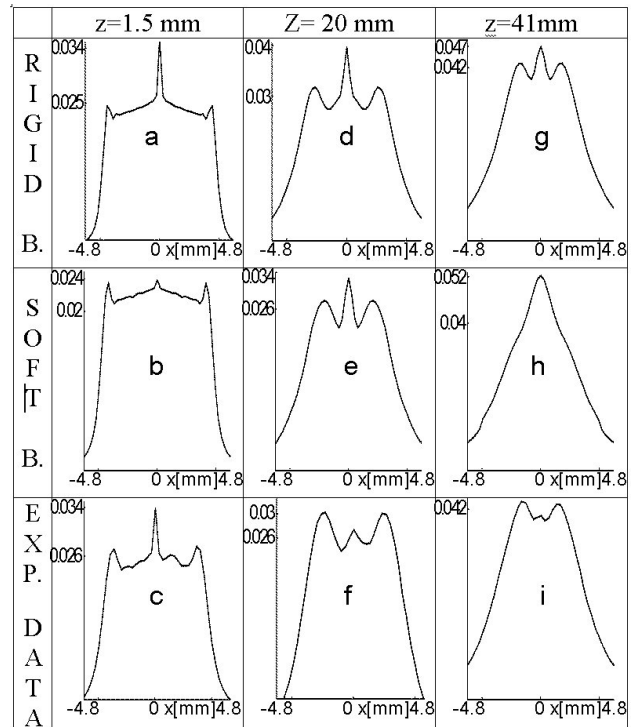


FIGURE 10. Theoretical and experimental  $P_{rms}$  parameter calculations of a 5 MHz transducer.

and c) the amplitude difference between the maxima and the following minima. A completely different pressure profile is found at  $z = 41$  mm, in Fig. 8g. It shows two well defined main lobes symmetrical to  $x = 0$  mm, while in Fig. 8h the pressure intensity is concentrated in one lobe around  $x = 0$  mm. The two main lobes, plotted in Fig. 8g, and a single lobe in Fig. 8h, are due to the fact that edge and direct waves are in-phase, so their amplitudes are added. The experimental intensity distribution plotted in Fig. 8i consists of two main lobes as in Fig. 8 g.

### 5.2.2. Peak-to-peak acoustic pressure

The theoretical and experimental results are plotted in Fig. 9. From a general comparison of the pressure distribution amplitudes between all cases, it can be said that the rigid baffle amplitude and the experimental readings are larger than the one computed for the soft baffle boundary condition. Also the rigid baffle data and the experimental measurements show a lower contribution of the edge and direct waves at  $x = 0$ , than the contribution of edge wave at  $x \approx a$ , while the opposite pattern was found for a soft baffle boundary condition. Then the amplitude and pressure distribution profiles of the experimental data tend to behave more like the computed acoustic pressure distribution when rigid baffle is considered as boundary condition.

### 5.2.3. Root-mean-squared acoustic pressure

Figure 10 shows the acoustic power for several observation points. The maximum amplitude, computed numerically, is

located at  $x = 0$ , due to the fact that direct and edge waves are added constructively (see Figs. 10a, 10b, 10d, 10e, 10g and 10h). The main differences between the numerical values produced by the two boundary conditions are: a) the amplitude difference between the main maxima to the following minima is larger for the rigid baffle case, and b) when the observation point is very close to the transducer, the maximum power is concentrated around  $x = 0$  mm as plotted in Fig. 10a, while in Fig. 10b it increases across the  $x$  direction until  $x = 0$  mm, where the maximum value is located. The experimental readings (see Figs. 10a, 10f and 10i) show a good agreement with the rigid baffle case, with the exception of the missing peaks at  $x = 0$  mm (Figs. 10f and 10i). Possible explanations are: a) when scanning at fixed positions the hydrophone did not acquire the signal at which the maximum amplitude occurs or b) the transducer plane is not normal to the hydrophone axis.

## 6. Conclusions

A comprehensive study of the acoustic pressure distribution has been carried out for pulse-echo ultrasonic transducers of resonant frequencies of 3.5 MHz and 5 MHz. A simulation process was developed based on the impulse response method considering different boundary conditions: the velocity is zero at the boundary (rigid baffle) and the pressure becomes zero at the boundary (soft baffle).

The simulation is able to determine the acoustic pressure at any point in space. It also gives information of the localized maximum and minimum energy produced by the transducers and, gives an approximated behavior of the acoustic radiation within the near field of a circular transducer.

A comparison between experimental and theoretical data including peak, peak to peak and root mean squared parameters for each boundary condition was done. The pressure distributions of the transducers, when these parameters are computed for every boundary condition, show that the transducer at resonant frequency of 3.5 MHz has very similar behavior to a soft baffle situation, while the transducer at 5 MHz of resonant frequency is closer to the behaviour expected when immersed in a rigid baffle. The acoustical pressures of the two transducers spread in different ways, even though the only difference between them is the resonant frequency.

The pressure distributions when peak and peak-to-peak parameters were computed have the same profile but different amplitudes. Also, their maxima intensities are not located at  $x = 0$  mm, while the  $P_{rms}$  parameter calculations show that the power of the acoustical pressure is concentrated on the transducer normal axis ( $x = 0$  mm).

Finally, this work has demonstrated that simulation of the acoustical pressure distribution produced by a vibrating circular surface can be used as guideline to design ultrasonic transducers. Also, it gives the theoretical fundament to predict the effects on the pressure distribution when more than one pulsating surface is vibrating.

## Acknowledgements

The authors would like to thank to the National Council of Science and Technology (CONACYT-31959A), the México-Cuba program, the Ibero-American Ultrasonic Technology Network (MAGIAS-RITUL UNESCO: 3304-3307) and the National University of México (PAPIIT-IN105900). We also want to thank Mr Eliseo Díaz Nacar, Mr Nelson Castillo Col-lazo and Mr Francisco Cárdenas Flores for their technical assistance.

- 
1. G.S. Kino, *Acoustic waves: devices, imaging and analog signal processing* (Prentice-Hall, Inc., New Jersey, 1987).
  2. A.J. Hayman and J.P. Wight, *J. Acoust. Soc. Am.* **66** (1979) 945.
  3. L.L. Beranek, *Acoustics* (McGraw-Hill, New York 1954).
  4. G.H. Harris, *J. Acoust. Soc. Am.* **70** (1981) 10.
  5. P.R. Stepanishen, *J. Acoust. Soc. Am.* **49** (1971) 1629.
  6. P.R. Stepanishen and G. Fisher, *J. Acoust. Soc. Am.* **69** (1981) 1610.
  7. F. Oberhettinger, *J. Res. Natl. Bur. Stand. (U.S.)* **B65** (1961).
  8. J.C. Lockwood and J.G. Willette, *J. Acoust. Soc. Am.* **53** (1973) 735.
  9. P.M. Morse and K.U. Ingard, *Theoretical acoustics* (McGraw-Hill, New York, 1968).
  10. D. Guyomar and J. Powers, *J. Acoust. Soc. Am.* **77** (1985) 907.
  11. B. Delannoy, H. Lasota, C. Bruneel, R. Torguet, and E. Bridoux, *J. of App. Phys.* **50** (1979) 5189.
  12. F.J. Rodríguez López, A. Ramos Fernández, J.L. San Emeterio Prieto, and E. Riera Franco de Sarabia, *An. Fís.* **89** (1993) 25.